Full Length Article

Ultra-Sensitive water detection based on NaErF$_4$@NaYF$_4$ high-level-doping upconversion nanoparticles

Jing Zuo [a], Wei Wang [b], Dongxu Zhang [e], Xikun Wang [a], Yanling Ma [a], Peitong Li [a], Yifan Li [a], Wen Sun [a], Youlin Zhang [c], Langping Tu [c,*], Yulei Chang [c,*], Qiqing Li [d,*], Hong Zhang [d,*]

[a] *Key Laboratory of Automobile Materials (Ministry of Education), College of Materials Science and Engineering, Jilin University, 130025 Changchun, China*
[b] *Department of Neurosurgery, The First Hospital of Jilin University, 130000 Changchun, China*
[c] *State Key Laboratory of Luminescence and Applications, Changchun Institute of Optics, Fine Mechanics and Physics, Chinese Academy of Sciences, 130033 Changchun, China*
[d] *Van 't Hoff Institute for Molecular Sciences, University of Amsterdam, Science Park 904, 1098 XH Amsterdam, the Netherlands*
[e] *Yinuoke Medicine Science and Technology Company, 130000 Changchun, China*

ARTICLE INFO

ABSTRACT

Water-sensitive detection plays a vital role in our society and life, such as the chemical industry, environmental monitoring, and food inspection. In this work water sensitivity as high as 5 ppm (0.0005 vol%) is realized based on a novel upconversion nanophosphor. Different from the popularly employed low-doping strategies, an efficient high-level-doping nanostructure, *i.e.*, NaErF$_4$@NaYF$_4$, is tailored for the desired upconversion emission, resulting in more than one order of magnitude enhancement of the sensitivity compared to the record of the low-doped counterparts. The superiority of this structure is determined to come from the robust interactions between the Er^{3+} ions and the water molecules adsorbed on the particle surface. This design offers a new strategy of nanophosphor structures for ultrasensitive water sensing and sheds light on further optimization of nanophosphor based sensors.

1. Introduction

Lanthanide (Ln^{3+}) ions doped upconversion nanoparticles (UCNPs) capable of converting near-infrared (NIR) light to ultraviolet–visible region have been demonstrated as promising luminescent materials for diverse applications, ranging from imaging and therapy to lasing and detection, *etc*. [1–16] Recently, they also have emerged as a kind of promising luminescent sensor for water detection, [17,18] which is of vital importance in fields like chemical industries, environmental monitoring, and food inspection [19–21]. Compared with the traditional Karl Fischer titration or electrochemical methods, [22] the spectroscopy-based detection approach has its superiority, such as non-contact, real-time, fast response, and easy preparation [23–27]. Among the reported luminescent probes, organic materials and organic–inorganic hybrid materials have shown high sensitivity but suffer from relatively weak reusability and stability, which arises great interest in developing inorganic luminescent sensors [28,29]. Especially, UCNPs stand out from the inorganic luminescent sensors as a competitive candidate since the Ln^{3+} possesses rich energy levels and long lifetimes,

which, in theory, can be easily affected by surrounding water molecules. The detection principle of UCNPs relies on the interaction between Ln^{3+} and water molecules, thus usually leads to the relevant luminescence quenching [30].

Up to date, two generations of UCNPs-based water sensors have been developed. The first generation was represented by ligand-free NaYF$_4$:20 %Yb, 2% Er bare core UCNPs as demonstrated by Huang and coworkers, where the detection limit (LOD) was down to 80 ppm (*i. e.* 0.008 vol%) in N, N-dimethylformamide (DMF) [17]. The inherent weakness of this sort of material is that unsatisfactory excitation wavelength (~980 nm), where relatively strong water absorption may lead to an overheating effect and being harmful to the detection accuracy. To avoid the overheating effect, the alternative was to shift the excitation wavelength to ~ 800 nm via introducing Nd^{3+} as a co-sensitizer, [18] which requires a core–shell structure of the UCNPs to prevent the strong quenching effect of Nd^{3+} towards the activator ions (such as Er^{3+}, Tm^{3+}, and Ho^{3+}) [5,31–34]. However, such construction (*e.g.* NaYF$_4$:Yb, Er@Yb, Nd or NaYF$_4$:Yb, Er@Yb, Nd@Y) obstructs the energy transfer between activators (*e.g.* Er^{3+}) and water molecules, and

---

* Corresponding authors.

E-mail addresses: tulangping@163.com (L. Tu), yuleichang@ciomp.ac.cn (Y. Chang), q.li@uva.nl (Q. Li), h.zhang@uva.nl (H. Zhang).

the LOD remained at ~ 100 ppm [18].

In recent years, a novel upconversion (UC) nanostructure, *i.e.* hexagonal $NaErF_4@NaYF_4$ had been proposed [35–37]. Benefitted from the well-ladder like energy levels of Er^{3+} and the high-level doping strategy, $NaErF_4@NaYF_4$ has the ability to efficiently convert the excitation of ~800, ~ 980, and ~1530 nm into visible UC emission. Subsequently, this newly designed nanostructure exhibits its huge potential in many fields, such as multi-mode bio-imaging, solar energy utilization, and UC emission spectra tuning [9,10,38–42]. However, so far, little attention had been paid to its capability in trace water detection.

In this work, we confirmed that compared with the traditional low-doped nanoparticles, the $NaErF_4@NaYF_4$ high-level-doping UC structure not only provides an alternative for ~800 nm excited detection, but also allows the LOD of water in DMF solvent to go down to 5 ppm, over one order of magnitude lower than the best-reported record of the traditional co-doped UC probes. Spectroscopy study reveals this improvement comes from the unique UC luminescence processes in this structure, typically (1) the extremely efficient energy migration between Er^{3+} ions easily bridges the activators and the emission quenchers, *i.e.,* water molecular adsorbed on the particle surface, (2) the abundant energy levels of Er^{3+} offers richer quenching paths and stronger quenching effects than those sensitizer ions (*e.g.,* Yb^{3+}), and (3) the thickness of the $NaYF_4$ shell is also critical to the sensing performance, which is optimized to 2 nm in our scenario. These results not only prove the applicability of $NaErF_4@NaYF_4$ nanostructures for trace water sensing, but also provide in-depth understanding of the Ln^{3+} UC process in the water environment.

2. Materials and methods

2.1. Reagents

$YCl_3 \cdot 6H_2O$, $ErCl_3 \cdot 6H_2O$, Oleic acid (OA, 90%), 1-octadecene (ODE, 90%), oleylamine (OM, 70%), CF_3COONa, $(CF_3COO)_3Y$ were purchased from Sigma-Aldrich. anhydrous DMF, methanol, ethanol, acetone, cyclohexane, NaOH, NH_4F were purchased from GFS Chemical. All the chemicals were purchased in analytical grade and used without further purification.

2.2. Preparation of core and core/shell upconversion nanoparticle

The preparation of core/shell upconversion nanoparticles consists of three steps: 1) synthesis of bare core, 2) prepare shell precursor, and 3) shell coating.

2.2.1. Synthesis of $NaErF_4$ and $NaYF_4$:20 %Yb, 2 %Er bare core structure

Typically, 1 mmol $ErCl_3 \cdot 6H_2O$ was added into a three-neck flask containing 6 mL OA and 15 mL ODE. In order to dissolve the solid $ErCl_3 \cdot 6H_2O$, the mixture was stirred at 160 ℃ for 30 min with argon protection and turned into a clear pink-colored solution. After cooled down to room temperature, the pink solution was added with 2.5 mmol NH_4F and 4 mmol NaOH dissolved in 5 mL methanol solution and it quickly turned into opacity. Then the mixture was heated and kept at 70 ℃ for 20 min to remove methanol molecules completely. Protected by argon flows, the methanol-free solution was heated rapidly and kept at 300℃ with stirring for a 90 min reaction. After three-times centrifuging (acetone once, and then ethanol twice), the as-obtained nanoparticles were dispersed in 4 mL cyclohexane. The $NaYF_4$:20 %Yb, 2 %Er nanoparticles were prepared with the same procedure and the $ErCl_3 \cdot 6H_2O$ is replaced with the corresponding rare earth chloride.

2.2.2. Synthesis of $NaYF_4$ and $NaYF_4$:20 %Nd, 10 %Yb precursor

In a typical procedure, 1 mmol CF_3COONa and 1 mmol $(CF_3COO)_3Y$ were added into a three-neck flask containing 6 mL OA, 15 mL ODE, and 6 mL OM. Under the argon atmosphere, the mixture was kept at 160 ℃ for 30 min with robust stirring to dissolve the solid reagents. Without a

cooling process, the mixture was directly heated to 290 ℃ for 1 h reaction. After cooling down, the obtained precursor was centrifuged with ethanol once, then redispersed in 4 mL ODE. The $NaYF_4$:20 %Nd, 10 % Yb precursor is prepared with the same procedure and the $(CF_3COO)_3Y$ is replaced with the corresponding rare earth fluoride.

2.2.3. Synthesis of $NaErF_4@NaYF_4$ and $NaYF_4$:20 %Yb, 2 %Er@ $NaYF_4$:20 %Nd, 10 %Yb core shell structure

2 mL cyclohexane with 0.5 mmol as-obtained $NaErF_4$ bare core nanoparticles were added into a three-neck flask containing 6 mL OA and 15 mL ODE. Under the protection of argon flows, the mixture was then heated directly to 300℃ with stirring for further reaction. As soon as the temperature reaches 300℃, a certain amount of $NaYF_4$ precursor was injected into the heated solution, reacting for 45 min to form a layer of $NaYF_4$ outside the $NaEF_4$ bare core nanoparticle. The shell thickness of $NaYF_4$ mainly depended on the amount of injected $NaYF_4$ precursor. After the reaction, the solution was cooled down to room temperature. The reactant nanoparticles were washed three times (acetone once, and then ethanol twice), and finally dispersed in 4 mL cyclohexane. The $NaYF_4$:20 %Yb, 2 %Er@ $NaYF_4$:20 %Nd, 10 %Yb core–shell nanoparticles were prepared with the same procedure and the $NaErF_4$ core and the $NaYF_4$ precursor were replaced with the corresponding $NaYF_4$:20 %Yb, 2 %Er core and $NaYF_4$:20 %Nd, 10 %Yb precursor.

2.3. Preparation of ligand-free nanoparticle

20 mg OA-UCNPs dispersed in 4 mL cyclohexane were mixed with a solution of $NOBF_4$ (20 mg in 4 mL Dichloromethane) and was stirred at room temperature overnight. The ligand-free UCNPs were obtained by centrifugation and then washed with toluene, and finally dispersed in DMF.

2.4. Characterization

The transmission electron microscopy (TEM) measurement was conducted on a Tecnai G2 F20 S-TWIN D573 electron microscope operated at 300 kV TEM. The powder X-ray diffraction (XRD) characterization was performed on an X-ray powder diffractometer with Cu Kα radiation (λ = 1.542 Å). The FTIR spectra of UCNPs with different surface ligands were examined by a Termo NICOLET6700 Fourier transform infrared spectrometer (FTIR) at room temperature. The upconversion steady-state emission spectra were collected at room temperature by FLS980 (Edinburgh Instruments). All the luminescence dynamics were recorded with a 500 MHz Tektronix digital oscilloscope and the excitation was realized by a nanosecond pulse from an optical parametric oscillator. During the spectroscopic measurements, all the samples were dispersed in cyclohexane or DMF with the same concentration of nanoparticles.

3. Results

The $NaErF_4$ bare core and $NaErF_4@NaYF_4$ core–shell UCNPs were synthesized via a co-precipitation method [43]. TEM images in Fig. 1a, b confirmed the uniformed morphology and size of these samples. Specifically, the diameters of core and core–shell nanoparticles were measured as 18.0 ± 0.6 nm and 22 ± 1.1 nm, respectively. Therefore, the $NaYF_4$ shell thickness of the core–shell sample can be calculated as ~ 2.0 nm. In addition, the pure hexagonal phase of these nanoparticles was testified by the XRD results (Figure S1). To make the particle hydrophilic, the oleophilic surface ligands of UCNPs (*i.e.,* OA, short for oleic acid molecules) were then removed. The nanoparticles were treated with nitrosoniumtetrafluoroborate ($NOBF_4$) according to the previous report. After the treatment, the UCNPs were dispersed well either in DMF or water. Fourier transform infrared spectrum (FTIR) of the UCNPs further confirmed the successful removal of the surface ligands. The characteristic peaks of OA molecules at 2860 cm^{-1}
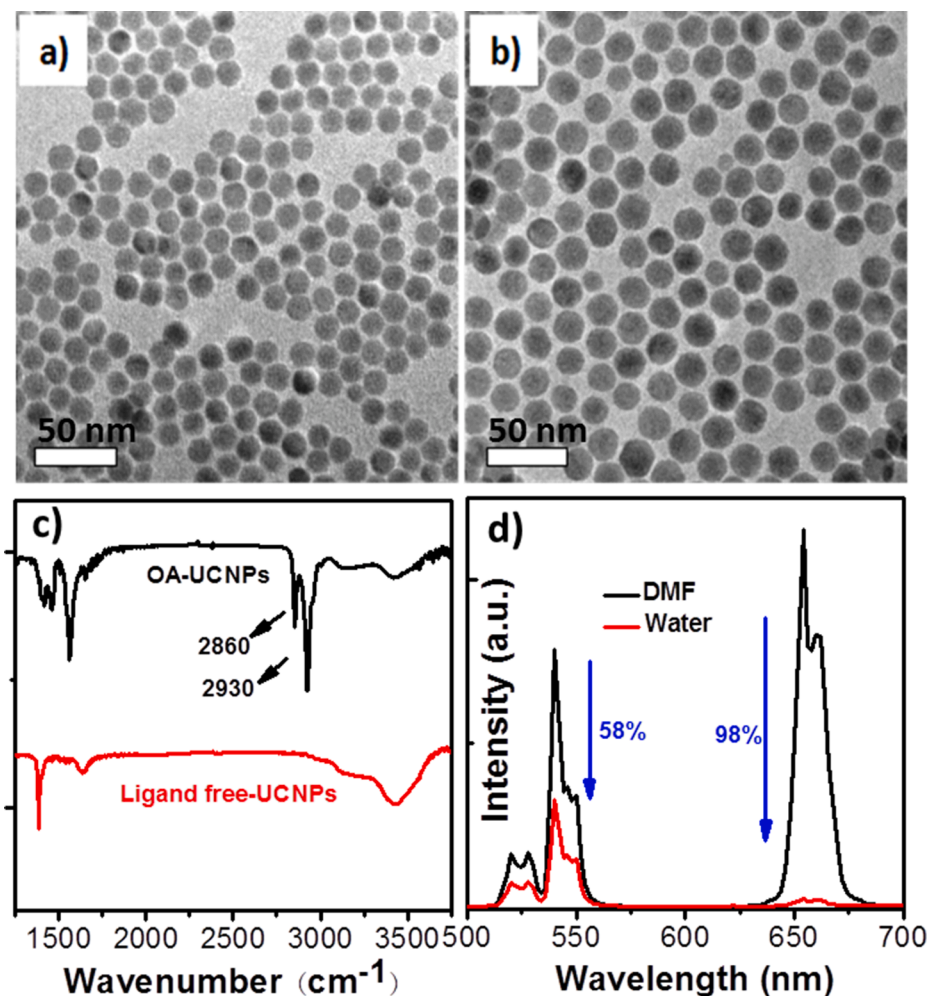
Fig. 1. The TEM images of (a) the NaErF$_4$ bare core nanoparticle and (b) the NaErF$_4$@NaYF$_4$ core–shell nanoparticle. (c) The Fourier transform infrared spectrum (FTIR) of the UC nanoparticles before (black line) and after (red line) the removal of the surface ligands (oleic acid molecules). (d) The UC emission spectra of NaErF$_4$@NaYF$_4$ core–shell nanoparticle in the DMF (black line) and pure water (red line) solvent, respectively. The samples were excited by an 800 nm laser, with a power density of 5 W/cm^2.

(symmetric stretching vibration of methylene) and 2930 cm^{-1} (asymmetric stretching vibration of methylene) completely disappeared after the treatment in Fig. 1c. After that, the emission spectra of the bare core and core/shell UCNPs in DMF solvent were recorded under 800 nm excitation, shown in Figure S2. The extremely weak UC emission of NaErF$_4$ bare core is due to the surface defects [35–37]. On the contrary, coating an inert shell of ~2.0 nm thickness to form NaErF$_4$@NaYF$_4$ core–shell UCNPs increased the UC luminescence greatly (peaking at ~520/545 nm and ~655 nm), correspondingly to the transitions of ^{2}H$_{11/2}$/^{4}S$_{3/2}$→^{4}I$_{15/2}$ and ^{4}F$_{9/2}$→^{4}I$_{15/2}$ of Er^{3+}, respectively (Fig. 1d). The choice of ~2 nm shell aimed to open the door to a certain extent for sensing the surface-relevant quenchers (discussed in the following text). Indeed, the UC emission of NaErF$_4$@NaYF$_4$ UCNPs was vulnerable to water, 58% quenching of green emission and 98% quenching of red emission in pure water compared with that in DMF (Fig. 1d). The robust variation suggested that the NaErF$_4$@NaYF$_4$ is a suitable candidate for water sensors.

To testify the water sensitivity, we compared the NaErF$_4$@NaYF$_4$ structure with the traditional Nd^{3+}/Yb^{3+} co-sensitized structure, which is another widely used UC structure under the 800 nm excitation (*i.e.*, NaYF$_4$: 20% Yb, 2% Er@NaYF$_4$: 10% Yb, 20% Nd), shown in Fig. 2a. To exclude the potential difference induced by different morphology/ structure of reference sample, we ensured these two samples with similar core (~18 nm) and shell (~2.0 nm) sizes (Figure S3). As displayed in Fig. 2b-d, the UC emission of NaErF$_4$@NaYF$_4$ nanoparticle under 800 nm excitation is quenched more severely than that of the traditional nanostructure, especially for the red emission band. Taking the situation of 1 vol% water as an example, the red emission of

NaErF$_4$@NaYF$_4$ UCNPs is quenched to 21% of its intensity in pure DMF solvent. In the meantime, the green/red UC emissions of Nd^{3+}/Yb^{3+} co-sensitized UCNPs decrease slightly to 85–88% (Fig. 2d).

The superior sensitivity of NaErF$_4$@NaYF$_4$ structure can be ascribed to the following factors: Firstly, benefited from the "fully doped" Er^{3+} ions in the core area, the energy migration among Er^{3+} is very efficient. Therefore, the excited states of Er^{3+} in the core area are very easy to migrate to the core–shell interface and finally quenched by the water molecules adsorbed at the particle surface (Fig. 3a). Secondly, different from the traditional systems where the major source of energy loss comes from the energy quenching of relatively highly doped Yb^{3+} ions. In the current high-level-doping system, Er^{3+} owns more abundant energy levels (compared with Yb^{3+}), endowing this Er^{3+}-rich system with much more processes to transfer corresponding energy to water (more excited energy levels of Er^{3+} may involve in the water quenching processes, while Yb^{3+} only has one excited energy level within the interesting range) and thus makes the potential energy quenching more efficient (Fig. 3b). The variation of down-shifting luminescence lifetimes further indicates that the Er^{3+}–H$_2$O interaction strength is also larger than that of Yb^{3+}–H$_2$O, even in the presence of low-doped case (*i.e.*, only doped 20% active Ln^{3+} in the core, Figure S4). Thirdly, it should be noticed that in the previous reports, the sum of UC intensity (*i.e.*, green emission plus red emission) is usually selected as the sensing referent. However, we find that for the NaErF$_4$@NaYF$_4$ structure, the quenching effect of green/red bands differs significantly. Being more specific, red emission is quenched to a much larger degree compared with the green one, especially in the case of trace water content (Fig. 2d). Therefore, taking the red emission as the referent can further improve the detection
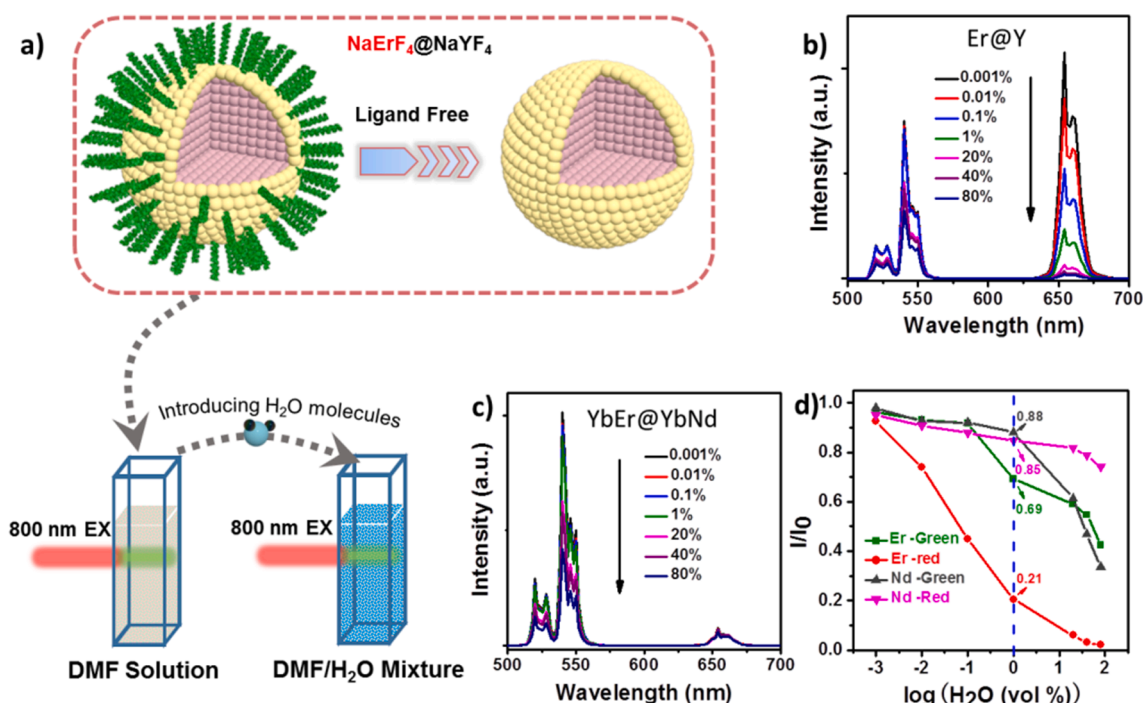
Fig. 2. (a) Schematic diagram of the UC luminescence-based water detection process. The UC emission spectra of (b) $NaErF_4@NaYF_4$ nanostructure and (c) $NaYF_4$: 20% Yb, 2% Er@$NaYF_4$: 10% Yb, 20% Nd traditional nanostructure in DMF solvent containing different amount of water (water contents are marked as volume percentages). Excitation is at 800 nm with a power density of 5 W/cm^2. (d) The corresponding relative UC emission intensities calculated as I/I_0 where I_0 is the emission intensity without water (the testing range of water content is 0.001% − 80%).

sensitivity. The difference of green/red bands relies much on the unique UC processes in $NaErF_4@NaYF_4$ system. As shown in Fig. 3c, due to the up-closed ion-to-ion distance, a non-neglectable source of red emission in $NaErF_4@NaYF_4$ is the energy migration assistant green → red CR processes. As a result, the additional energy quenching processes during the green → red CR make the red emission band exhibits a higher "sensitivity" to the water content.

Next, the $NaErF_4$ inner core size (Figure S5) and $NaYF_4$ shell thickness were also found to play important roles in pursuing a sensitive detector (the uniformed morphology of series particles with different shell thicknesses are shown in Figure S6). From the previous reports, [18,28] the UC quenching data for a certain water content can be linearly fitted according to the following equation:

$$I/I_0 = C + klog[H_2ovol\%] \qquad (1)$$

Then, the limit of detection (LOD) could be calculated following the mathematical expression:

$$LOD = 10^\wedge(3\sigma/K) \qquad (2)$$

where σ is the standard deviation of the percentage of I/I_0, and K is the calibration plot slope, which can be obtained from the variation of UC emission intensity versus different water contents.

According to Eq.(A.2), the inert shell (*i.e.*, $NaYF_4$) plays a conflict role in the detection. On one hand, a thicker shell is conducive to high sensitivity, because it is conducive to obtain a relatively small σ value by providing a stronger and more stable UC emission signal. As shown in Fig. 4, the σ value decreased from 0.230 to 0.065 with the shell thickness increased from 2 to 5.5 nm. On the other hand, thick shells also play a negative role by expanding the interaction distance between the activator (Er^{3+}) and the surface quencher (water molecules). As a result, under the premise of high sensitivity detection (water content is lower than 0.005 vol%), the absolute value of K decreases from 0.21 to 0.07 as the shell thickness increases (Fig. 4b). However, if the shell thickness is too thin, *e.g.,* 0.5–1 nm, based on our experiment condition (emission spectra are collected at room temperature by equipment Edinburgh

Instruments FLS980, excited by 800 nm with power density 5 W/cm^2), the UC emission intensity is extremely weak, which also brings a significantly enhanced σ value and hinders the efforts of obtaining an ideal LOD (Figure S7). Therefore, the tradeoff resulted in the optimal shell thickness located to 2 nm in the current scenario, and the corresponding LOD was determined to be as low as 5 ppm (*i.e.,* 0.0005%). It is worth noticing that the contrast sample (*i.e.,* $NaYF_4$: 20% Yb, 2% Er@$NaYF_4$: 10% Yb, 20% Nd nanostructure) performs a much larger LOD value (85 ppm, Figure S8) under the same experimental conditions, which highlights the advantage of the new structure.

To further elucidate the working mechanism of water detection, luminescence dynamics investigation of the optimized ligand-free $NaErF_4@NaYF_4$ nanostructure (core diameter: 18 nm and shell thickness: 2 nm) is necessary. Since the lifetime of UC emission is subject to complex intermediate processes and cannot reflect the depopulation process of each energy level directly [44,45]. We focused on the down-shifting luminescence. As shown in Fig. 5 and Table S1, the lifetimes of every monitored excited level gradually decrease as the water content increases, indicating that the UC emission quenching is induced by the simultaneous energy transfer from the five energy states of Er^{3+} (*i.e.,* $^4S_{3/2}$, $^4F_{9/2}$, $^4I_{9/2}$, $^4I_{11/2}$ and $^4I_{13/2}$) to water molecules. It should be noticed that even the water content is at a relatively low level (such as 0–0.1 vol%), the non-neglectable lifetime variation of each energy state can still be clearly observed, which agrees well with the ultra-sensitivity results observed from the steady-state spectroscopic measurements (Fig. 4b). Finally, as a proof of concept, we purchased DMF solvents from two different companies, and examined their water impurity via our strategy. It is quite gratifying to notice that the experimental results are well in line with the manufacturers' instructions (Table S2).

4. Conclusions

In summary, a new strategy of highly sensitive detection of trace water is proposed and validated using high-level-doping UCNPs (*i.e.,* $NaErF_4@NaYF_4$). Taking the red UC emission as referent, the limit of
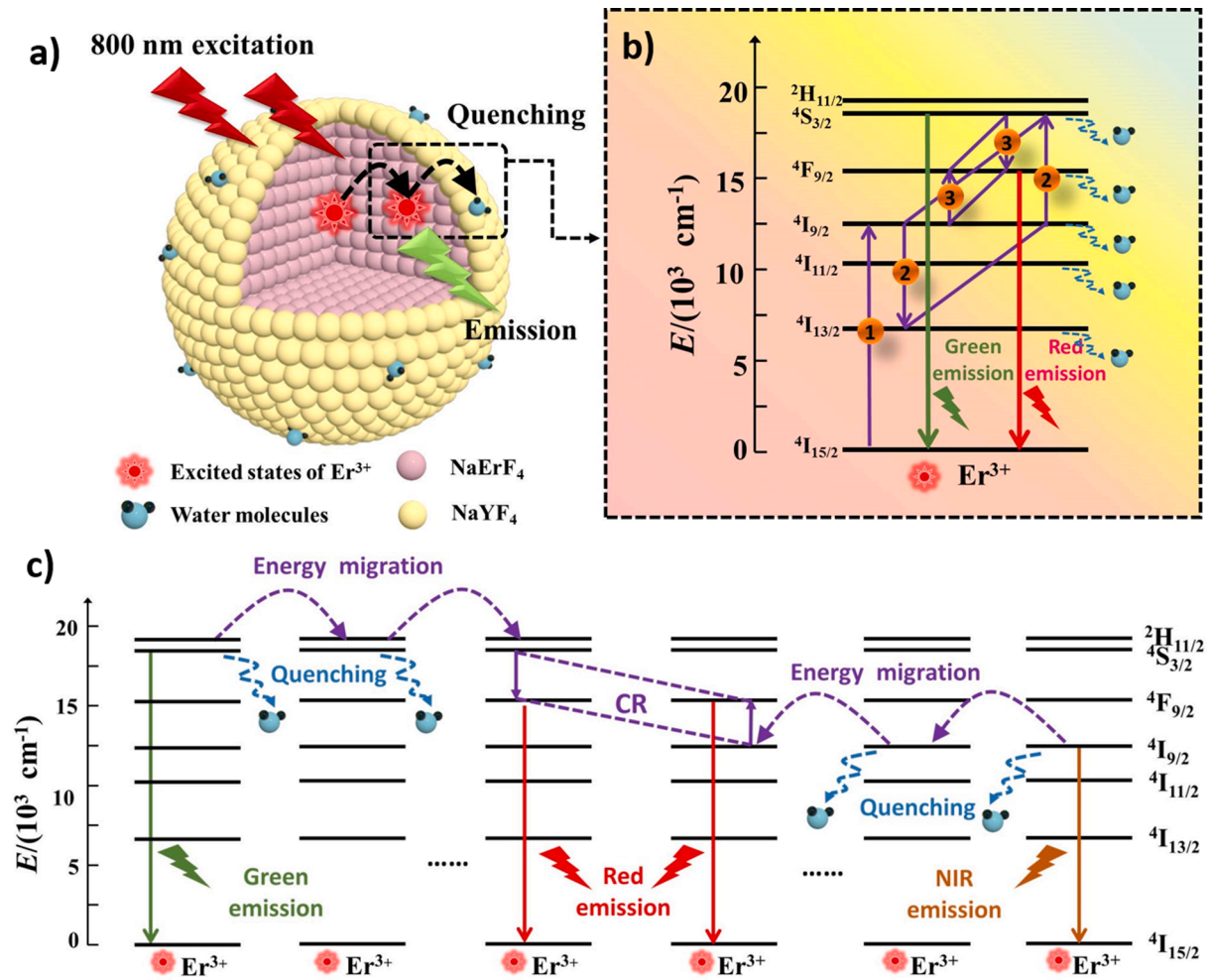
Fig. 3. (a) The energy migration assisted UC luminescence quenching processes (from NaErF$_4$@NaYF$_4$ core–shell nanoparticles to water molecules). (b) Schematic representation of the UC processes and the potential energy quenching paths in NaErF$_4$@NaYF$_4$ core–shell nanoparticles. (c) Schematic representation of the energy quenching during the energy migration assistant green → red cross-relaxation processes.
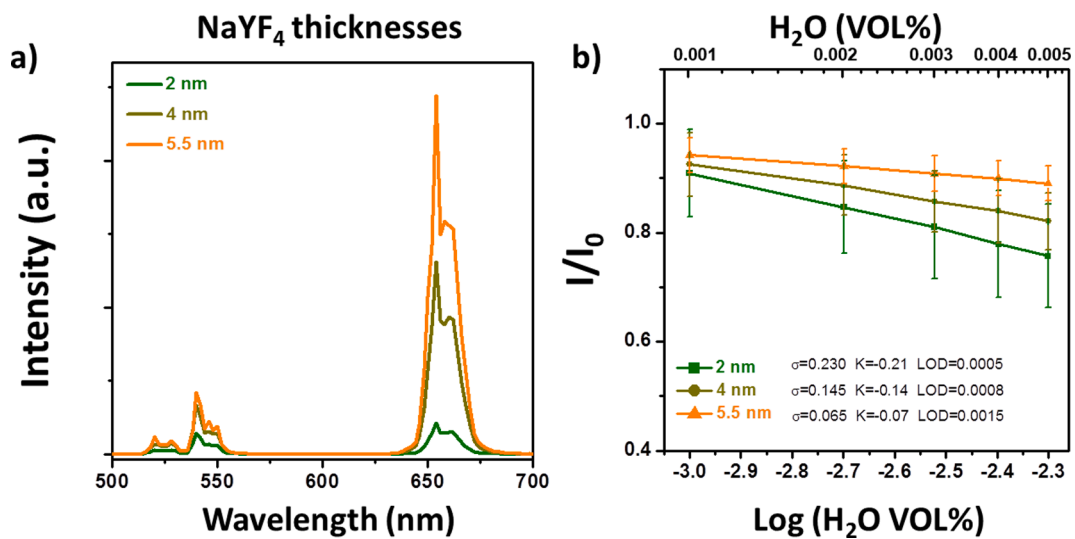

Fig. 4. (a) The shell-thicknesses dependent UC emission spectra of NaErF$_4$@NaYF$_4$ core–shell nanoparticles in DMF solvent (excited by 800 nm, 5 W/cm^2). (b) Water dependence of the red UC emission intensity for ligand-free NaErF$_4$@NaYF$_4$ core–shell nanoparticles, where water content varies from 0.001 to 0.005 vol% in DMF solvent (I_0 is the solution emission intensity without water). The NaYF$_4$ shell thicknesses are 2 nm (green), 4 nm (brown), and 5.5 nm (bright yellow), respectively. The emission intensity here is the integration from 580 to 700 nm. Excitation is at 800 nm with a power density of 5 W/cm^2.
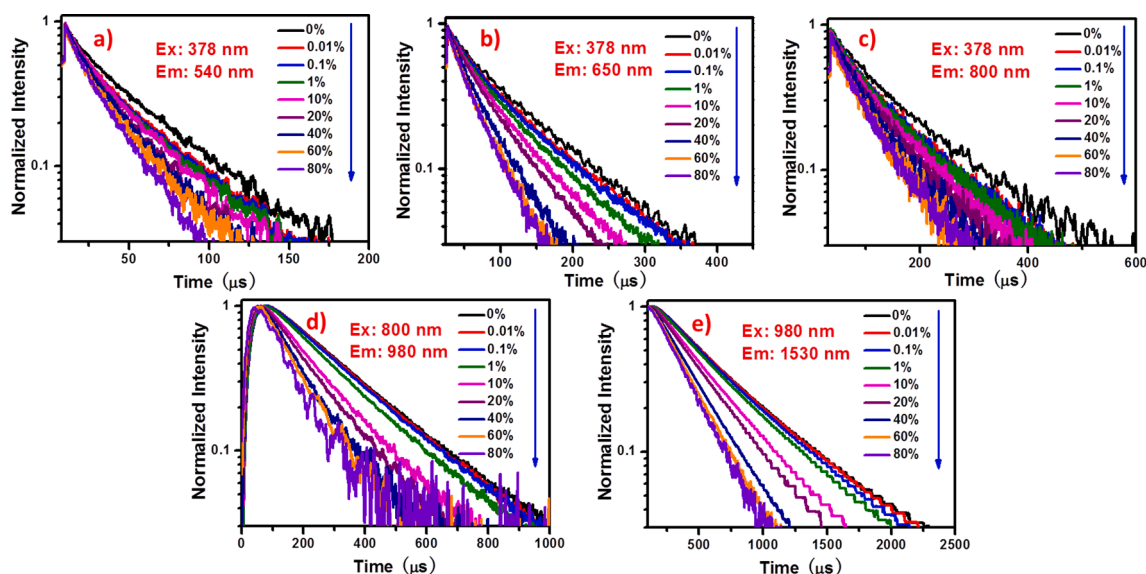
Fig. 5. Luminescence decay curves of ligand-free NaErF$_4$@NaYF$_4$ nanostructure dispersed in DMF solvent containing different water contents. (a-c) Decay curves of 540, 650, and 800 nm emission of Er^{3+}, respectively, with excitation at 378 nm. (d) Decay curves of 980 nm emission of Er^{3+} with excitation at 800 nm. (e) Decay curves of 1530 nm emission of Er^{3+} with excitation at 980 nm.

water detection in DMF solution reach unprecedentedly small to 5 ppm, over one order of magnitude compared with the traditional co-doped UC probes. The improvement is discussed to come from the unique properties of NaErF$_4$@NaYF$_4$ UCNPs. Firstly, the robust excitation energy migration among Er^{3+} ions enables the quenching effect of water to affect Er^{3+} ions in the core effectively. Secondly, richer energy levels and stronger interaction strength make Er^{3+} suffer a larger quenching effect (from water molecules) than traditional sensitizer ions (*e.g.,* Yb^{3+}). Finally, the shell thickness is optimized to ~2 nm to balance the testing standard deviation (σ) and the absolute magnitude of the calibration plot slope (K). Our findings provide not only a valuable strategy for highly sensitive water detection but also a better understanding of the Ln^{3+} upconversion mechanism.

Declaration of Competing Interest

The authors declare that they have no known competing financial interests or personal relationships that could have appeared to influence the work reported in this paper.

Acknowledgment

Appendix A. Supplementary data

Supplementary data to this article can be found online at https://doi.org/10.1016/j.apsusc.2021.151701.

References

[1] F. Wang, D. Banerjee, Y. Liu, X. Chen, X. Liu, Upconversion nanoparticles in biological labeling, imaging, and therapy, Analyst 135 (2010) 1839–1854.
[2] G. Chen, C. Yang, P.N. Prasad, Nanophotonics and nanochemistry: Controlling the excitation dynamics for frequency up- and down-conversion in lanthanide-doped Nanoparticles, Acc. Chem. Res. 46 (2013) 1474–1486.
[3] J. Zuo, L. Tu, Q. Li, Y. Feng, I. Que, Y. Zhang, X. Liu, B. Xue, L.J. Cruz, Y. Chang, H. Zhang, X. Kong, Near infrared light sensitive ultraviolet-blue nanophotoswitch for imaging-guided "Off-On" therapy, ACS Nano 12 (2018) 3217–3225.
[4] J. He, W. Zheng, F. Ligmajer, C.F. Chan, Z. Bao, K.L. Wong, X. Chen, J. Hao, J. Dai, S.F. Yu, D.Y. Lei, Plasmonic enhancement and polarization dependence of nonlinear upconversion emissions from single gold nanorod@SiO$_2$@CaF$_2$:Yb^{3+}, Er^3$^+$ hybrid core-shell-satellite nanostructures, Light Sci, Appl. 6 (2017), e16217.
[5] B. Liu, C. Li, P. Yang, Z. Hou, J. Lin, 808-nm-light-excited lanthanide-doped nanoparticles: rational design, luminescence control and theranostic applications, Adv. Mater. 29 (2017) 1605434.
[6] F. Wang, S. Wen, H. He, B. Wang, Z. Zhou, O. Shimoni, D. Jin, Microscopic inspection and tracking of single upconversion nanoparticles in living cells, Light Sci. Appl. 7 (2018) 18007.
[7] M. Haase, H. Schaefer, Upconverting nanoparticles, Angew. Chem. Int. Edit. 50 (2011) 5808–5829.
[8] Y. Zhuang, D. Chen, W. Chen, W. Zhang, X. Su, R. Deng, Z. An, H. Chen, R.-J. Xie, X-ray-charged bright persistent luminescence in NaYF$_4$:Ln^{3+}@NaYF$_4$ nanoparticles for multidimensional optical information storage, Light Sci. Appl. 10 (2021) 132.
[9] Y. Zhang, X. Zhu, Y. Zhang, Exploring heterostructured upconversion nanoparticles: from rational engineering to diverse applications, ACS Nano 15 (2021) 3709–3735.
[10] S. Zha, H.F. Chau, W.Y. Chau, L.S. Chan, J. Lin, K.W. Lo, W.C.S. Cho, Y.L. Yip, S. W. Tsao, P.J. Farrell, L. Feng, J.M. Di, G.L. Law, H.L. Lung, K.L. Wong, Dual-targeting peptide-guided approach for precision delivery and cancer monitoring by using a safe upconversion nanoplatform, Adv. Sci. 8 (2021) 2002919.
[11] R. Weinstain, T. Slanina, D. Kand, P. Klan, Visible-to-NIR-light activated release: from small molecules to nanomaterials, Chem. Rev. 120 (2020) 13135–13272.
[12] A. Steinegger, O.S. Wolfbeis, S.M. Borisov, Optical sensing and imaging of pH values: spectroscopies, materials, and applications, Chem. Rev. 120 (2020) 12357–12489.
[13] X. Shan, F. Wang, D. Wang, S. Wen, C. Chen, X. Di, P. Nie, J. Liao, Y. Liu, L. Ding, P. J. Reece, D. Jin, Optical tweezers beyond refractive index mismatch using highly doped upconversion nanoparticles, Nat. Nanotechnol. 16 (2021) 531–537.
[14] Y. Feng, Z. Li, Q. Li, J. Yuan, L. Tu, L. Ning, H. Zhang, Internal OH$^-$ induced cascade quenching of upconversion luminescence in NaYF$_4$:Yb/Er nanocrystals, Light Sci. Appl. 10 (2021) 105.
[15] Y. Zhou, W. Chen, J. Zhu, W. Pei, C. Wang, L. Huang, C. Yao, Q. Yan, W. Huang, J. S.C. Loo, Q. Zhang, Inorganic-organic hybrid nanoprobe for NIR-excited imaging of hydrogen sulfide in cell cultures and inflammation in a mouse model, Small 10 (2014) 4874–4885.
[16] Y.i. Zhou, W. Pei, C. Wang, J. Zhu, J. Wu, Q. Yan, L. Huang, W. Huang, C. Yao, J.S. C. Loo, Q. Zhang, Rhodamine-modified upconversion nanophosphors for ratiometric detection of hypochlorous acid in aqueous solution and living cells, Small 10 (17) (2014) 3560–3567.
[17] S. Guo, X. Xie, L. Huang, W. Huang, Sensitive water probing through nonlinear photon upconversion of lanthanide-doped nanoparticles, ACS Appl. Mater. Interfaces 8 (1) (2016) 847–853.
[18] D. Chen, M. Xu, P. Huang, M. Ma, M. Ding, L. Lei, Water detection through Nd^{3+}-sensitized photon upconversion in core-shell nanoarchitecture, J. Mater. Chem. C 5 (22) (2017) 5434–5443.
[19] W.-E. Lee, Y.-J. Jin, L.-S. Park, G. Kwak, Fluorescent actuator based on microporous conjugated polymer with intramolecular Stack structure, Adv. Mater. 24 (41) (2012) 5604–5609.

[20] L. Chen, J.W. Ye, H.P. Wang, M. Pan, S.Y. Yin, Z.W. Wei, L.Y. Zhang, K. Wu, Y. N. Fan, C.Y. Su, Ultrafast water sensing and thermal imaging by a metal-organic framework with switchable luminescence, Nat. Commun. 8 (2017) 15985.

[21] E.D. Tsamis, J.N. Avaritsiotis, Design of planar capacitive type sensor for "water content" monitoring in a production line, Sens. Actuator A Phys. 118 (2005) 202–211.

[22] Y.Y. Liang, Automation of Fischer Karl water titration by flow-injection sampling, Anal. Chem. 62 (1990) 2504–2506.

[23] N. Hildebrandt, K.D. Wegner, W.R. Algar, Luminescent terbium complexes: Superior Forster resonance energy transfer donors for flexible and sensitive multiplexed biosensing, Coord. Chem. Rev. 273 (2014) 125–138.

[24] J. Zhang, F. Cheng, J. Li, J.J. Zhu, Y. Lu, Fluorescent nanoprobes for sensing and imaging of metal ions: Recent advances and future perspectives, Nano Today 11 (2016) 309–329.

[25] Z. Liu, C. Shang, H. Ma, M. You, An upconversion nanoparticle-based photostable FRET system for long-chain DNA sequence detection, Nanotechnology 31 (2020), 235501.

[26] Y. Li, C. Deng, N. Sun, Hydrophilic probe in mesoporous pore for selective enrichment of endogenous glycopeptides in biological samples, Anal. Chim. Acta 1024 (2018) 84–92.

[27] W. He, M. You, Z. Li, L. Cao, F. Xu, F. Li, A. Li, Upconversion nanoparticles-based lateral flow immunoassay for point-of-care diagnosis of periodontitis, Sens. Actuator B Chem. 334 (2021) 129673, https://doi.org/10.1016/j. snb.2021.129673.

[28] Q. Deng, Y. Li, J. Wu, Y. Liu, G. Fang, S. Wang, Y. Zhang, Highly sensitive fluorescent sensing for water based on poly(m-aminobenzoic acid), Chem. Commun. 48 (24) (2012) 3009, https://doi.org/10.1039/c2cc17856g.

[29] N.C. Shaner, M.Z. Lin, M.R. McKeown, P.A. Steinbach, K.L. Hazelwood, M. W. Davidson, R.Y. Tsien, Improving the photostability of bright monomeric orange and red fluorescent proteins, Nat. Methods 5 (6) (2008) 545–551.

[30] R. Arppe, I. Hyppänen, N. Perälä, R. Peltomaa, M. Kaiser, C. Würth, S. Christ, U. Resch-Genger, M. Schäferling, T. Soukka, Quenching of the upconversion luminescence of $NaYF_4:Yb^{3+}$, Er^{3+} and $NaYF_4:Yb^{3+}$, Tm^{3+} nanophosphors by water: the role of the sensitizer Yb^{3+} in non-radiative relaxation, Nanoscale 7 (27) (2015) 11746–11757.

[31] Y.F. Wang, G.Y. Liu, L.D. Sun, J.W. Xiao, J.C. Zhou, C.H. Yan, Nd^{3+}-sensitized upconversion nanophosphors: Efficient in vivo bioimaging probes with minimized heating effect, ACS Nano 7 (2013) 7200–7206.

[32] Q. Min, J. Lei, X. Guo, T. Wang, Q. Yang, D. Zhou, X. Yu, S.F. Yu, J. Qiu, Q. Zhan, X. Xu, Atomic-level passivation of individual upconversion nanocrystal for single particle microscopic imaging, Adv. Funct. Mater. 30 (2020) 1906137.

[33] Y. Zhong, G. Tian, Z. Gu, Y. Yang, L. Gu, Y. Zhao, Y. Ma, J. Yao, Elimination of photon quenching by a transition layer to fabricate a quenching-shield sandwich Structure for 800 nm excited upconversion luminescence of Nd^{3+} sensitized nanoparticles, Adv. Mater. 26 (2014) 2831–2837.

[34] J. Mo, L. Shen, Q. Xu, J. Zeng, J. Sha, T. Hu, K. Bi, Y. Chen, An Nd^{3+}-sensitized upconversion fluorescent sensor for epirubicin detection, Nanomaterials 9 (2019) 1700.

[35] N.J.J. Johnson, S. He, S. Diao, E.M. Chan, H. Dai, A. Almutairi, Direct evidence for coupled surface and concentration auenching dynamics in lanthanide-doped nanocrystals, J. Am. Chem. Soc. 139 (2017) 3275–3282.

[36] J. Zuo, Q. Li, B. Xue, C. Li, Y. Chang, Y. Zhang, X. Liu, L. Tu, H. Zhang, X. Kong, Employing shells to eliminate concentration quenching in photonic upconversion nanostructure, Nanoscale 9 (23) (2017) 7941–7946.

[37] Q. Chen, X. Xie, B. Huang, L. Liang, S. Han, Z. Yi, Y.u. Wang, Y. Li, D. Fan, L. Huang, X. Liu, Confining excitation energy in Er^{3+}-sensitized upconversion nanocrystals through Tm^{3+}-mediated transient energy trapping, Angew. Chem. Int. Edit. 56 (26) (2017) 7605–7609.

[38] X. Zhu, X. Liu, H. Zhang, M. Zhao, P. Pei, Y. Chen, Y. Yang, L. Lu, P. Yu, C. Sun, J. Ming, I.M. Ábrahám, A.M. El-Toni, A. Khan, F. Zhang, High-fidelity NIR-II multiplexed lifetime bioimaging with bright double interfaced lanthanide nanoparticles, Angew. Chem. Int. Edit. 60 (44) (2021) 23545–23551.

[39] W. Wang, Z. Feng, B. Li, Y. Chang, X.u. Li, X.u. Yan, R. Chen, X. Yu, H. Zhao, G. Lu, X. Kong, J. Qian, X. Liu, Er^{3+} self-sensitized nanoprobes with enhanced 1525 nm downshifting emission for NIR-IIb in vivo bio-imaging, J. Mater. Chem. B 9 (12) (2021) 2899–2908.

[40] T. Wang, Y.i. Li, L. Yan, Q. Liang, X.u. Wang, J. Tao, J. Yang, Y. Qiu, Y. Meng, B. Mao, S. Zhao, P. Zhou, B.o. Zhou, Core-shell $NaErF_4@NaYF_4$ upconversion nanoparticles qualify as a NIR speckle wavemeter for a visible CCD, Nanoscale 13 (38) (2021) 16207–16215.

[41] Z. Sun, H. Huang, R. Zhang, X. Yang, H. Yang, C. Li, Y. Zhang, Q. Wang, Activatable rare earth near-infrared-II fluorescence ratiometric nanoprobes, Nano Lett. 21 (2021) 6576–6583.

[42] D.i. Liu, X. Zhang, W. Qin, B. Yao, L. Tu, Y. Li, G. Wang, H. Luan, X. Kong, Z. Ding, Y. Jiang, H. Zhao, Z. Zhang, L. Zhang, Influence of $NaErF_4@NaYF_4$ nanoparticles doping on performances of $Cu_2ZnSn(S, Se)_4$ solar cell, Sol. Energy Mater. Sol. Cells 203 (2019) 110175, https://doi.org/10.1016/j.solmat.2019.110175.

[43] N.J.J. Johnson, A. Korinek, C. Dong, F.C.J.M. van Veggel, Self-focusing by Ostwald ripening: A strategy for layer-by-layer epitaxial growth on upconverting nanocrystals, J. Am. Chem. Soc. 134 (2012) 11068–11071.

[44] J. Zuo, D. Sun, L. Tu, Y. Wu, Y. Cao, B. Xue, Y. Zhang, Y. Chang, X. Liu, X. Kong, W. J. Buma, E.J. Meijer, H. Zhang, Precisely tailoring upconversion dynamics via energy migration in core-shell nanostructures, Angew. Chem. Int. Edit. 57 (2018) 3054–3058.

[45] L. Tu, X. Liu, F. Wu, H. Zhang, Excitation energy migration dynamics in upconversion nanomaterials, Chem. Soc. Rev. 44 (2015) 1331–1345.